

Development of transition edge superconducting bolometers for the SAFARI Far-Infrared spectrometer on the SPICA space-borne telescope

Philip Mauskopf^a, Dmitry Morozov^a, Dorota Glowacka^b, David Goldie^b, Stafford Withington^b,
Marcel Bruijn^c, Piet DeKorte^c, Henk Hoevers^c, Marcel Ridder^c, Jan Van Der Kuur^c,
Jian-Rong Gao^d

^aSchool of Physics and Astronomy, Cardiff University, Queens Buildings, Cardiff CF24 3AA,
Wales, UK;

^bCambridge University Astrophysics Group, Cavendish Laboratory, JJ Thomson Avenue,
Cambridge, CB3 0HE, UK

^cSpace Research Institute of the Netherlands, Sorbonnelaan 2, 3584 CA Utrecht, Netherlands

^dKavli Institute of Nanoscience, Faculty of Applied Sciences, Delft University of Technology,
Lorentzweg 1, 2628 CJ Delft, Netherlands

ABSTRACT

We describe the optimization of transition edge superconducting (TES) detectors for use in a far-infrared (FIR) Fourier transform spectrometer (FTS) mounted on a cryogenically cooled space-borne telescope (e.g. SPICA). The required noise equivalent power (NEP) of the detectors is approximately 10^{-19} W/ $\sqrt{\text{Hz}}$ in order to be lower than the photon noise from astrophysical sources in octave wide bands in the FIR. The detector time constants must be less than 10 ms in order to allow fast scanning of the FTS mechanism. The detectors consist of superconducting thermometers suspended on thin legs of thermally isolating silicon nitride and operate at a temperature of approximately 100 mK. We present the design of the detectors, a proposed focal plane layout and optical coupling scheme and measurements of thermal conductance and time constant for low NEP prototype TES bolometers.

Keywords: bolometer, transition-edge superconductor, far-infrared

1. INTRODUCTION

The far-infrared (FIR) band from 1-10 THz (30 – 300 μm) is only accessible from space and contains half of the energy radiated by material since recombination. This radiation is primarily from dust and gas that absorbs starlight and reradiates at longer wavelengths. Measurements of this radiation are particularly important for detailed studies of star formation both in nearby galactic molecular clouds and in distant galaxies at high redshift. Even though there is a peak in the intensity of radiation at these wavelengths, the amount of power from distant sources is small and therefore requires sensitive detectors.

Future FIR space missions such as SPICA,¹ SPIRIT,² SPECS,³ and FIRI⁴ will require detectors with sensitivities of $\leq 10^{-19}$ W/ $\sqrt{\text{Hz}}$. In this paper, we describe the design of transition edge superconducting bolometers for the SAFARI (formerly ESI) instrument⁵ on the SPICA telescope. SPICA is a Japanese-led mission to fly a 3 metre diameter IR telescope with cryogenically cooled ($\simeq 5$ K) optics. Cooling the optics eliminates the background radiation that limits the sensitivity of ambient temperature FIR space telescopes such as HERSCHEL.⁶ The loading is then dominated by astrophysical background sources. In the FIR, the dominant source is the Zodiacal light, scattered sunlight from diffuse particles in the solar system.

Further author information: (Send correspondence to P. D. Mauskopf)
P. D. Mauskopf.: E-mail: mauskopf@astro.cf.ac.uk, Telephone: +44 2920 876 170

FTS band (μm)	Background loading (fW)	Photon NEP at detector ($\text{aW}/\sqrt{\text{Hz}}$)	Array size
35-60	0.4-0.8	2-3	64×64
60-110	0.3-0.7	1.5-2.5	32×32
110-210	0.4-0.6	1.5-2	20×20

Table 1. SAFARI focal plane parameters

The SAFARI instrument is an imaging Fourier Transform Spectrometer (FTS) with three bands covering the wavelength ranges: $35 - 60\mu\text{m}$, $60 - 110\mu\text{m}$ and $110 - 210\mu\text{m}$. The loading in these bands is estimated to be dominated by emission from the Zodiacal light at a level of $0.3 - 1 \text{ fW}$.⁵ This gives a photon noise equivalent power (NEP) at the detectors of $1 - 3 \times 10^{-18} \text{ W}/\sqrt{\text{Hz}}$. Therefore, we require detectors with electrical NEPs at least 3 times lower than the photon noise limit, i.e. $\leq 3 \times 10^{-19} \text{ W}/\sqrt{\text{Hz}}$. The requirement for the response time of the detectors for SAFARI is set to $\tau \leq 10 \text{ ms}$ by the maximum scanning speed of the FTS mechanism and the downlink bandwidth.

There are several different types of detectors under development for potential use on the SAFARI instrument including semiconductor photoconductors, transition edge superconducting (TES) bolometers, silicon bolometers and kinetic inductance detectors. In this paper, we describe the status of the design and testing of silicon nitride suspended TES bolometers for SAFARI.

Silicon nitride suspended bolometers were originally developed for ground-based mm-wave observations and have been used in a large number of ground-based and sub-orbital experiments such as SuZIE,⁷ BOLO-CAM/AzTEC,⁸ BOOMERANG.^{9,10} In addition, silicon nitride suspended bolometers are integrated into the HERSCHEL-SPIRE⁶ instrument and the PLANCK-HFI¹¹ instrument both due to be launched by ESA in the near future. All of the detectors in these instruments use as the sensitive element germanium thermistor chips that are bonded to the silicon nitride membranes in a hybrid process.^{12,13}

More recently, a number of groups have developed bolometers incorporating silicon nitride thermal isolation combined with TES thermometers (see¹⁴ and references therein). These devices have significant advantages over the germanium-based bolometers: i) lower heat capacity and decreased response time due to strong electrothermal feedback, ii) ability to fabricate large arrays using standard thin film photolithography, iii) ability to read out large numbers of pixels using a low-power SQUID multiplexed readout. These detectors along with multiplexed SQUID readouts are currently in use in a number of ground-based and balloon-borne instruments including SCUBA2, APEX-SZ, EBEX, CLOVER and SPIDER.

2. DETECTOR DESIGN

The theoretical performance of a TES bolometer is determined by the thermal conductance of the support legs, G , the heat capacity of the absorber and superconducting thermometer, C , the superconducting transition temperature, T_c , and the loop gain of the electrothermal feedback, L_0 .¹⁴ The baseline design for the SAFARI TES detectors is similar to the design of TES detectors for longer wavelengths incorporating a thermally isolated silicon nitride membrane supporting a free space absorber with dimensions of approximately $1.5\lambda \times 1.5\lambda$ and a TES thermometer with dimensions of approximately $100\mu\text{m} \times 100\mu\text{m}$.

The sensitivity of a bolometer is given by:

$$\text{NEP} = \sqrt{\gamma 4kT^2G} \quad (1)$$

where γ is a number between 0.5 and 1 depending on the difference between the base temperature and the transition temperature of the superconductor and the dependence of the thermal conductance on temperature. Ground-based and balloon-borne mm-wave instruments require detectors with sensitivities on the order of $\text{NEP} \simeq 10^{-17} \text{ W}/\sqrt{\text{Hz}}$. In order to achieve sensitivities two orders of magnitude lower, we have to fabricate devices with extremely thin mechanical suspension and operate at temperatures $\leq 100 \text{ mK}$. For a detector electrical NEP of $2 \times 10^{-19} \text{ W}/\sqrt{\text{Hz}}$ at an operating temperature of 100 mK , we require a thermal conductance of $G \leq 7 \times 10^{-14} \text{ W/K}$.

One way to achieve the low thermal conductance values required for SAFARI is by fabricating devices with very long and thin legs of silicon nitride. The thermal transport in insulators at low temperatures is through low energy vibrational and torsional mechanical (phonon) modes that depend on the geometry of the thermal link. The number of phonon modes present is proportional to T^D where D is the dimensionality of the thermal link - i.e. the number of dimensions of the silicon nitride leg larger than the phonon wavelength,

$$\lambda_{\text{phonon}} = \frac{hc_s}{kT} \quad (2)$$

At low temperatures where the thermal wavelength of the phonons is larger than the width or thickness of the silicon nitride legs the thermal conductance is dominated by the lowest 4 phonon modes which have a universal value for thermal conductance of:

$$G = 4g_0\eta \quad (3)$$

where $g_0 \simeq 1 \text{ pW/K} \times T$ and $\eta < 1$ is the transmission coefficient of the wire.¹⁵ For the sound speed in silicon nitride of 6200 m/s, the thermal phonon wavelength is $\lambda = 3\mu\text{m}$ at 100 mK so we expect legs with cross sectional area smaller than this to be close the 1-D limit.

If the transmission coefficient is dominated by reflections at discontinuities in the phonon waveguide at the ends of the legs but the mean free path of the phonons is longer than the legs then we would expect to see a thermal conductance that is independent of the length of the thermal link, $\eta \simeq A$. This is known as the ballistic or radiative regime. In the limit of random scattering at the surfaces where the phonon mean free path is much smaller than the length of the thermal link, the transmission coefficient is given by $\eta = \kappa A/L$. This is known as the diffuse scattering limit. In the case of 1-D transport where the maximum thermal conductance is given by the quantum conductance then $\eta = \lambda_{\text{mfp}}/L$ where λ_{mfp} is the mean free path of a phonon and L is the length of the thermal link.

The frequency response of a bolometer depends on the heat capacity of the absorber, the loop gain, L_0 and the thermal conductance, G of the legs:

$$\tau = \frac{C}{G} \frac{1}{1 + L_0} \quad (4)$$

2.1 Materials properties

The mean free path of the phonons in the legs is related to the thermal diffusivity by $\lambda_{\text{mfp}} = 3D/c_s$ where c_s is the sound speed in the medium and the diffusivity is:

$$D = \frac{G}{C_V} \frac{L}{A} \quad (5)$$

where L is the length of a thermal link, A is the cross sectional area and C_V is the heat capacity per unit volume. Silicon nitride has a room temperature diffusivity of $D \simeq 10^{-6} \text{ m}^2/\text{s}$ and $c_s \simeq 10000 \text{ m/s}$ so that the mean free path of the phonons is only 0.5 nm and the scattering time is $\tau \simeq 3 \times 10^{-14} \text{ s}$. In theory, the thermal conductivity and heat capacity have the same temperature dependence so that the mean free path of phonons should be independent of temperature. However, at low temperatures, the increase in the phonon wavelength means that the mean free path of phonons increases and large mean free paths ($> 100\mu\text{m}$) have been measured in silicon nitride 2-D membranes at $< 300 \text{ mK}$.¹⁶

The thermal conductance of long thin legs of silicon nitride has been studied experimentally by a number of groups^{15,17-21} using a variety of geometries including long straight legs, meandered legs and legs with nanometer scale constrictions. The measured phonon mean free path in silicon nitride nanowires is $\simeq 1\mu\text{m}$ at 4 K²² giving a thermal diffusivity of $D = 3 \times 10^{-3} \text{ m}^2/\text{s}$ which decreases as the temperature is lowered. The measured thermal conductivity of silicon nitride legs with sub-micron thickness and width shows a break in the temperature dependence corresponding to 1-D phonon transport below 100 mK.²¹

The heat capacity of a suspended silicon nitride membrane with a SiO passivation layer has been measured to be $C \simeq 200 \text{ fJ/K}$ for a volume of $140\mu\text{m} \times 200\mu\text{m} \times 1\mu\text{m}$ ²³ giving a specific heat of $C_V = 14 \text{ J/K/m}^3$ at 100 mK. This value is four orders of magnitude larger than the value computed from the bulk silicon nitride, either

Device	Leg $l \times w \times t$ (μm)	TES size $l \times w$ (μm)
3-1	$2490 \times 6 \times 1$	110×110
3-7	$1310 \times 6 \times 1$	110×110
4-3	$1830 \times 6 \times 1$	110×110
4-4	$1825 \times 11 \times 1$	110×110

Table 2. Dimensions of prototype devices. The TES size is close to 1.5λ for the shortest wavelength SAFARI band. The final size of the suspended island will be approximately twice the size of the TES.

$0.58T^3$ J/K/m³ (from Holmes, et al., 1998)¹⁸ or $0.66T^3$ J/K/m³ (from Moktadir, et al., 2002)²⁴ and 10 times higher than the estimated heat capacity of the metal heater and readout resistors deposited on the membrane. Zink and Hellman measure the specific heat of silicon nitride films with different underlayers (thermal silicon dioxide and low temperature oxide) and find a value for the specific heat at 4 K of about $6T^3$ J/K/m³ or ten times higher than the bulk value.²⁵ Fon, et al. measure a total heat capacity of 24.5 fJ/K for a $25\mu\text{m} \times 25\mu\text{m} \times 0.12\mu\text{m}$ membrane at 4.5 K for a specific heat of 330 J/K/m³ decreasing to $\simeq 7$ J/K/m³ at 0.5 K.²⁰

2.2 Prototype devices

In order to confirm previous measurements of the materials properties, we fabricated devices with suspended Ti/Au TES thermometers on silicon nitride membranes with comparable size to the dimensions required for SAFARI using a variety of leg geometries. Table 2.2 gives the detailed dimensions of the devices studied and figures 1 and 2 show photographs of two of the designs.

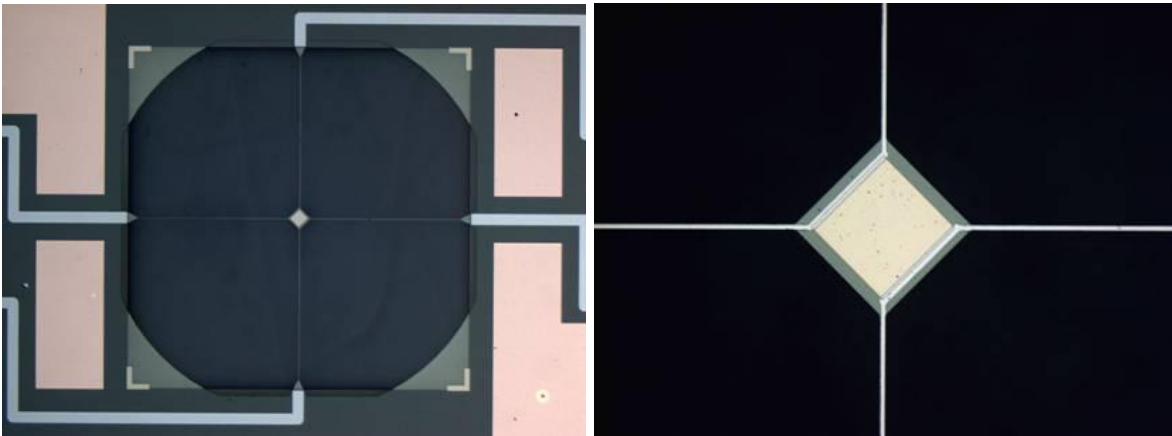


Figure 1. Photograph of the SPICA 3-7 TES and central part of the chip. The entire device is approximately 2.5 mm on a side. The silicon nitride legs are 1.31 mm long and $6 \mu\text{m}$ wide. The Ti/Au TES is $110 \times 110\mu\text{m}$.

We measured the thermal conductance and electrical response times of these silicon nitride suspended TES thermometers at a variety of critical temperatures using different TES thicknesses.

3. DEVICE CHARACTERIZATION

Devices were characterized in test facilities at SRON-Utrecht (dilution refrigerator), Cambridge (miniature dilution refrigerator) and Cardiff (double stage adiabatic demagnetization refrigerator (ADR)). We describe in detail measurements of the devices 3-7 and 3-1 at Cardiff.

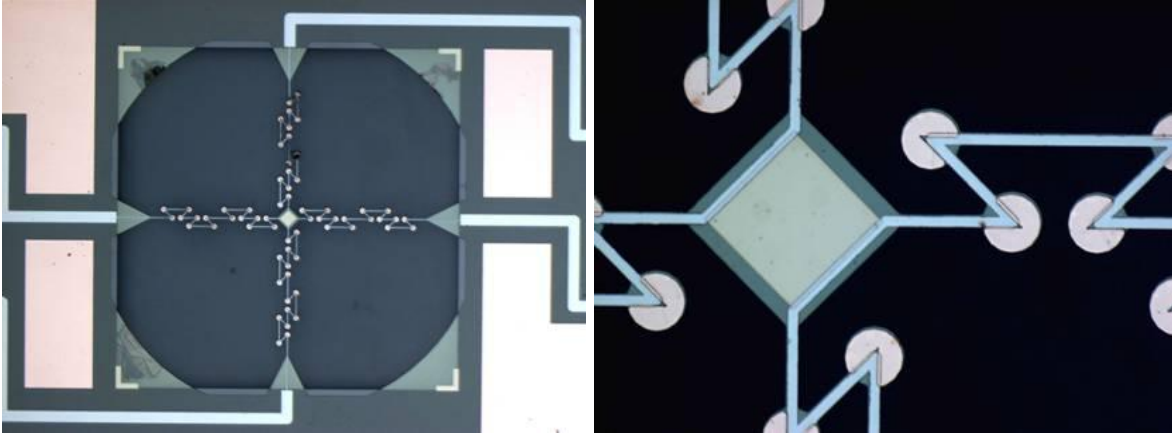


Figure 2. Photograph of the SPICA 3-1 TES and central part of the chip. The wiring is 90 nm thick Niobium. The legs are meandered with 135 degree bends. Initially copper dots were deposited at the vertex of the bends to scatter phonons but these were found not to be necessary and drastically increased the time constant.

3.1 IV curves

We used a NIST series array SQUID amplifier²⁶ mounted on the 1 K stage to measure the TES current-voltage (IV) characteristics as a function of base temperature. The readout circuit we used is a modified version of the Star-Cryo flux locked loop read-out electronics²⁷ with reduced gain on the preamplifier input stage. The cold TES circuit is shown in figure 3, where R_s is the shunt resistor, R_b is the bias resistor, L_{in} is the input coil of the SQUID and L_{FB} is the feedback coil of the SQUID. Note that the value $R_s = 5$ mOhm is given at room temperature and R_b is outside the cold part of the cryostat. For IV measurements $R_b = 200$ kOhm in series with ≈ 400 Ohm of wiring resistance.

Measured IV curves for the device 3-7 are shown on fig. 3. In order to record the IV data, V_b was rapidly ramped up and then held at a maximum voltage while the temperature of the ADR was increased to above the superconducting transition temperature. When the TES turned normal, the ADR was ramped back down to base temperature and then the bias voltage was ramped down at a much lower rate. The waveform period was about 200 sec.

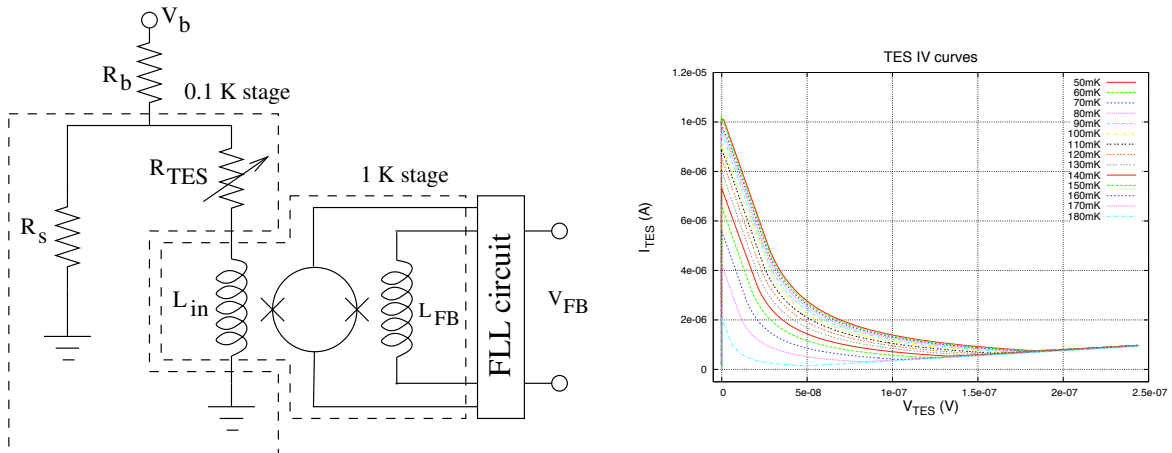


Figure 3. Left: TES read out circuit. Right: Current-voltage curves for device 3-7 at different base temperatures

When the TES is superconducting the full bias current $I_b = V_b/R_b$ is flowing through TES and SQUID input

coil. The SQUID system gain is computed from the superconducting part of the IV curve:

$$G_{\text{SQUID}} = \frac{V_{\text{FB}}}{I_{\text{b}}}. \quad (6)$$

The voltage on the TES terminals V_{TES} is given by:

$$V_{\text{TES}} = \left(I_{\text{b}} - \frac{V_{\text{FB}}}{G_{\text{SQUID}}} \right) \times R_{\text{s}} \quad (7)$$

where the TES current, $I_{\text{TES}} = V_{\text{FB}}/G_{\text{SQUID}}$ and $R_{\text{TES}} = V_{\text{TES}}/I_{\text{TES}}$ is the TES DC resistance. In this analysis we assume that

$$R_{\text{b}} \gg \frac{R_{\text{s}}R_{\text{TES}}}{R_{\text{s}} + R_{\text{TES}}}. \quad (8)$$

3.2 Thermal conductance measurements

The power dissipation in the TES, $P_{\text{TES}} = V_{\text{TES}}I_{\text{TES}}$ at different base temperatures as a function of TES bias is shown in figure 4. The temperature dependence of the power plateaus where the TES is on the superconducting

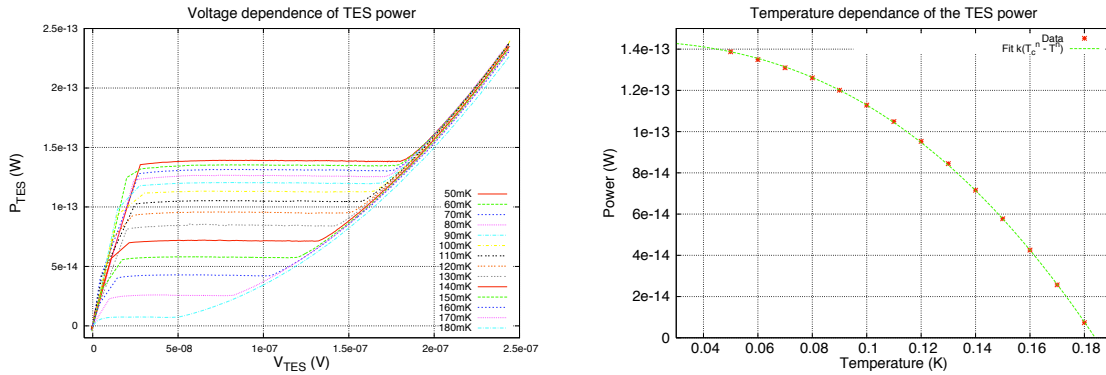


Figure 4. Left: Electrical power dissipated in TES 3-7 vs. applied voltage from the IV curves for different base temperatures. Right: Constant power level vs. base temperature for TES 3-7. The curve is a simple power law fit to the data with an index of $n = 2.5$.

transition is also shown in figure 4. The data are well fit by a single power law given by:

$$P_{\text{TES}} = k(T_c^n - T^n), \quad (9)$$

where k is a coefficient characterizing heat transfer. The thermal conductance, G , of the legs is equal to

$$G = \frac{dP}{dT} = knT^{n-1}, \quad (10)$$

After fitting the power vs. temperature data the values shown in Table 3 have been calculated for $T_c \simeq 200$ mK devices measured at Cardiff and SRON. Overall, we find a consistent power law index for the temperature dependence of the power dissipation of $n \simeq 2.6$ for all devices indicating that the phonon modes are not purely one-dimensional at these temperatures and geometries. In addition, the thermal conductance values scale with the ratio (wt/l) indicating that the thermal transport is diffusive rather than ballistic.

Device Measured	7-4-4 SRON	7-4-3 SRON	7-3-7 Cardiff	7-3-1 Cardiff
Leg $l \times w \times t$	$1825 \times 11 \times 1$	$1830 \times 6 \times 1$	$1310 \times 6 \times 1$	$2490 \times 6 \times 1$
T_c	168 mK	203 mK	184 mK	178 mK
k (W/K ^{<i>n</i>})	$(1.3 \pm 0.1) \times 10^{-11}$	$(4.9 \pm 0.1) \times 10^{-12}$	$(9.9 \pm 0.1) \times 10^{-12}$	$(7.7 \pm 0.1) \times 10^{-12}$
n	2.6 ± 0.1	2.6 ± 0.1	2.5 ± 0.1	2.8 ± 0.1
Thermal G (pW/K)	1.9	1.0	2.0	1.0
NEP _{phonon} (aW/ $\sqrt{\text{Hz}}$)	1.2	1.0	1.2	0.84
$\alpha = \frac{kl_n}{4wt}$ (W/K ^{<i>n</i>} /m)	1.4×10^{-3}	1.0×10^{-3}	1.3×10^{-3}	2.2×10^{-3}

Table 3. TES parameters for devices fabricated at SRON

3.3 Time constant measurements

The detector electrical time constants have been measured using a small amplitude pulsed square waveform on top of the DC bias point of the TES. We used a Tektronix DPO 7104 oscilloscope in AC coupling mode to record the time stream data. The time constant was computed by fitting an exponential decay to the time stream data. We measured the time constant at different bias points on the transition at the bath temperature $T_b = 100$ mK. The IV curve measured at $T = 100$ mK with corresponding time constant values is shown in figure 5. An example of a coadded time trace is also shown in figure 5. The slope in the time trace is due to the AC coupling at the input of the oscilloscope. Complex impedance measurements have also been done at SRON and the frequency response agrees with the time constant measurement. Complete analysis of the complex impedance measurements will be presented elsewhere.

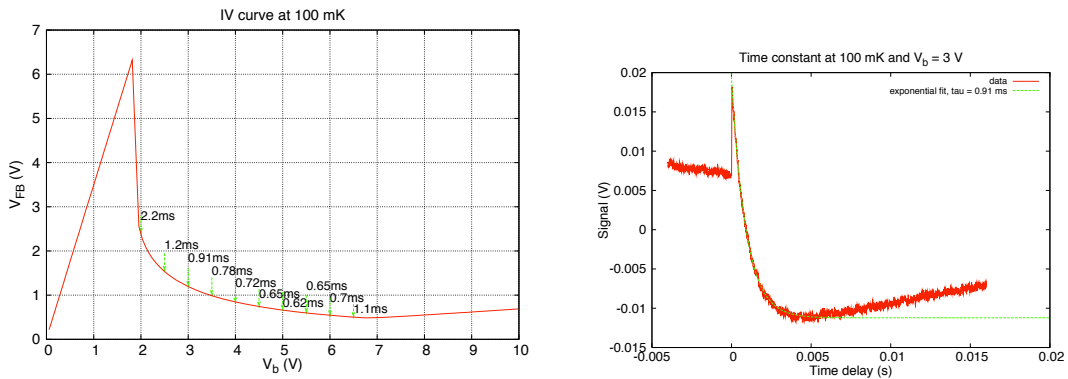


Figure 5. Left: Measured IV curve for bolometer 3-7 at $T = 100$ mK and mapped values of τ . Right: Coadded time trace with exponential fit to the response to a step bias.

The time constants for all of the devices measured in Table 3 range from 0.2 – 2 ms. From this data and from the $R(T)$ data for the TES, we can estimate the heat capacity of the suspended silicon nitride membrane and TES. For the device 3 – 7, we estimate a maximum loop gain of $L_0 = 40 - 50$. This combined with the minimum time constant of 0.62 ms and thermal conductance of 2 pW/K gives a heat capacity of 50-60 fJ/K. The estimated heat capacity of the Ti/Au TES at 180 mK is 36 fJ/K indicating a residual heat capacity of 10-20 fJ/K for the membrane corresponding to a heat capacity per unit volume of 0.7 J/K/m^3 .

Scaling these numbers to lower temperatures allows an estimate of the sensitivity and speed of response of a similar sized membrane at 100 mK. Scaling the thermal conductance according to the index, n for the same leg geometry at 100 mK gives $G(100 \text{ mK}) = 0.6 \text{ pW/K}$ and a projected $\text{NEP} = 6 \times 10^{-19} \text{ W}/\sqrt{\text{Hz}}$. Assuming that

the heat capacity is proportional to temperature and assuming the same loop gain, we would expect this device to have a time constant of $\tau = 0.4 - 1.2$ ms. Reducing the thermal conductance by a factor of 10 in order to achieve an NEP $\leq 2 \times 10^{-19}$ W/ $\sqrt{\text{Hz}}$ would give a projected detector time constant of 4-12 ms.

We have fabricated a second round of prototype devices with the same geometry but with a TES transition temperature of 80 mK. Initial testing of the first of these devices (geometry 3-7) gives a measured $G \simeq 0.16$ pW/K, estimated phonon NEP = 2×10^{-19} W/ $\sqrt{\text{Hz}}$ and a time constant of $\simeq 1$ ms.

4. OPTICAL COUPLING DESIGN

The SAFARI optics reimaging the sky at the output of the FTS onto a focal plane with a focal ratio $f \leq 20$. The focal plane array is specified to have Nyquist sampling of $f\lambda/2$ corresponding to pixel spacings of 480, 850 and 1600 μm . We have considered several different options for optical coupling to the TES detectors including a filled array of free space absorbers, an array of lenses feeding multimode antennas or absorbers and an array of feedhorns feeding multimode absorbers. Due to the requirement on thermal conductance at this time it does not seem possible to construct a filled array with enough mechanical strength to survive fabrication and launch. Lens arrays and horn arrays allow the sensitive element to be smaller than the pixel separation and leave room on the detector wafer for long thermally isolating legs which can be meandered around the central absorber.

The preliminary design for optical coupling of the detectors is to have multimoded horns feeding broad-band cavities with a matched free space absorber connected to the TES on the silicon nitride island. The design of the absorber cavity depends on the detailed design of the horn, mechanical mounting of the detector wafer and the substrate thickness. A schematic of a prototype single pixel horn coupled assembly is shown in figure 6.

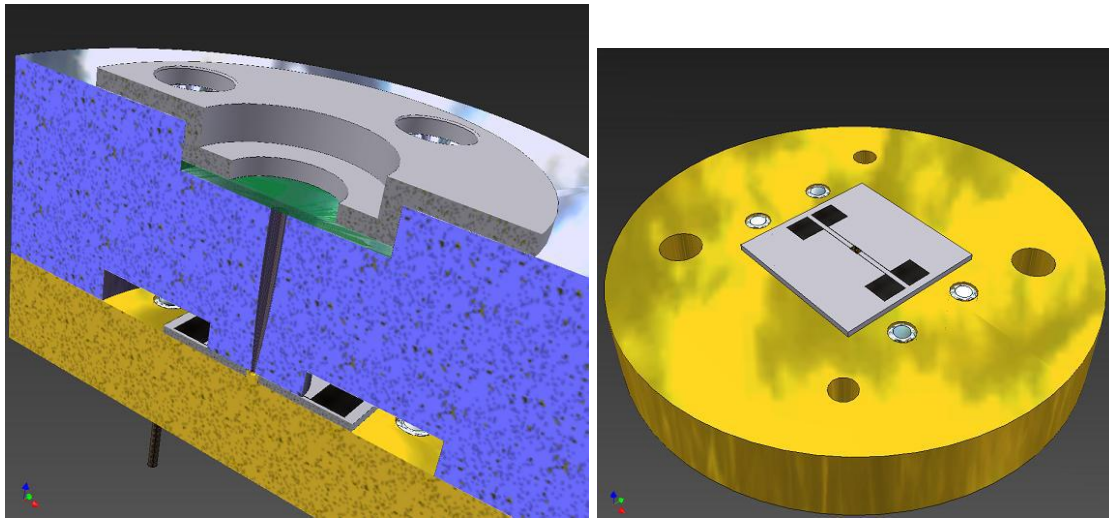


Figure 6. Design of a single pixel TES detector coupled to a multimode horn. The detector is mounted on a metal block containing a hemispherical cavity backshort and superconducting light tight feedthroughs for the readout signals.

5. CONCLUSIONS

We have begun an optimization of silicon nitride suspended TES bolometers for use in the SAFARI instrument on the SPICA IR telescope. We have characterized prototype devices with long thermally isolating legs of silicon nitride and transition temperatures of $\simeq 200$ mK and $\simeq 80$ mK. We find the thermal conductance of the legs to be approximated by a power law with an index of 2.6 over a temperature range from < 100 mK to 200 mK. We measure the time constants of the suspended TES thermometers to be 0.2 – 2 ms at 200 mK both from the response to a small bias step and in the frequency domain using complex impedance measurements. This corresponds to a heat capacity of 40-60 fJ/K and an electrothermal loop gain of 20-200. There is evidence that the transport down narrow silicon nitride wires is diffusive and the mean free path is $\simeq 1\mu\text{m}$ and only weakly

dependent of the cross sectional area of the wires. The total heat capacity of the suspended island is comparable to the calculated heat capacity of the TES and we do not see significant excess heat capacity from the silicon nitride membrane.

We are now in the process of designing and fabricating the first optical pixels with free space absorbers. Remaining challenges will be to achieve the required pixel spacing and low thermal conductance of the legs. A large amount of theoretical work has been done in the past several years on thermal conductivity in thin silicon nitride wires. Kuhn, et al. calculate the thermal conductivity of a narrow dielectric wire in the limit of scattering off of the rough edges to be given by $G \propto T^{n-1} = T^{1.5}$ at low temperatures, close to our measurement of $n = 2.6$.²⁸ Murphy, et al. calculate the thermal conductivity in the case where short wavelength phonons propagate in the diffuse regime while long wavelength phonons propagate ballistically.²⁹ In this case, there is a transition at low temperatures to quantum conductance proportional to temperature. Finally, a number of groups calculate the effects of introducing different types of structures as phonon filters to engineer the thermal conductance of small wires.³⁰⁻³⁴ Using these ideas, we plan to engineer devices with the required performance using support legs that are short enough to achieve the required pixel spacing for SAFARI.

ACKNOWLEDGMENTS

The authors acknowledge support in the UK from PPARC and in the Netherlands from SRON.

REFERENCES

- [1] H. Kaneda, T. Nakagawa, T. Onaka, T. Matsumoto, H. Murakami, K. Enya, H. Kataza, H. Matsuhara, and Y. Y. Yui, "Development of space infrared telescope for the SPICA mission," in *Optical, Infrared, and Millimeter Space Telescopes. Edited by Mather, John C. Proceedings of the SPIE, Volume 5487, pp. 991-1000 (2004).*, J. C. Mather, ed., *Presented at the Society of Photo-Optical Instrumentation Engineers (SPIE) Conference 5487*, pp. 991–1000, Oct. 2004.
- [2] D. Leisawitz, C. Baker, A. Barger, D. Benford, A. Blain, R. Boyle, R. Broderick, J. Budinoff, J. Carpenter, R. Caverly, P. Chen, S. Cooley, C. Cottingham, J. Crooke, D. DiPietro, M. DiPirro, M. Femiano, A. Ferrer, J. Fischer, J. Gardner, L. Hallock, K. Harris, K. Hartman, M. Harwit, L. Hillenbrand, T. Hyde, D. Jones, J. Kellogg, A. Kogut, M. Kuchner, B. Lawson, J. Lecha, M. Lecha, A. Mainzer, J. Mannion, A. Martino, P. Mason, J. Mather, G. McDonald, R. Mills, L. Mundy, S. Ollendorf, J. Pellicciotti, D. Quinn, K. Rhee, S. Rinehart, T. Sauerwine, R. Silverberg, T. Smith, G. Stacey, H. P. Stahl, J. Staguhn, S. Tompkins, J. Tveekrem, S. Wall, and M. Wilson, "The Space Infrared Interferometric Telescope (SPIRIT): mission study results," in *Space Telescopes and Instrumentation I: Optical, Infrared, and Millimeter. Edited by Mather, John C.; MacEwen, Howard A.; de Graauw, Mattheus W. M.. Proceedings of the SPIE, Volume 6265, pp. 626540 (2006).*, *Presented at the Society of Photo-Optical Instrumentation Engineers (SPIE) Conference 6265*, July 2006.
- [3] J. C. Mather, D. Leisawitz, and T. F.-I. I. M. S. W. Group, "The spirit and specs far-infrared / submillimeter interferometry missions," *The Institute of Space and Astronautical Science report. S.P. 14*, pp. 219–224, 20001200.
- [4] F. Helmich and R. Ivison, "FIRI - a Far-Infrared Interferometer," *ArXiv e-prints 707*, July 2007.
- [5] B. Swinyard, "Esi: the far-infrared instrument for the spica mission," *Space Telescopes and Instrumentation I: Optical, Infrared, and Millimeter 6265(1)*, p. 62650L, SPIE, 2006.
- [6] M. Griffin, A. Abergel, P. Ade, P. André, J.-P. Baluteau, J. Bock, A. Franceschini, W. Gear, J. Glenn, D. Griffin, K. King, E. Lellouch, D. Naylor, G. Olofsson, I. Perez-Fournon, M. Rowan-Robinson, P. Saraceno, E. Sawyer, A. Smith, B. Swinyard, L. Vigroux, and G. Wright, "Herschel-SPIRE: design, performance, and scientific capabilities," in *Space Telescopes and Instrumentation I: Optical, Infrared, and Millimeter. Edited by Mather, John C.; MacEwen, Howard A.; de Graauw, Mattheus W. M.. Proceedings of the SPIE, Volume 6265, pp. 62650A (2006).*, *Presented at the Society of Photo-Optical Instrumentation Engineers (SPIE) Conference 6265*, July 2006.
- [7] B. Benson, S. Church, P. Ade, J. Bock, K. Ganga, C. Henson, and K. Thompson, "Measurements of Sunyaev-Zel'dovich effect scaling relations for clusters of galaxies," *Astrophysical Journal 617*, pp. 829–846, DEC 20 2004.

- [8] G. W. Wilson, J. E. Austermann, T. A. Perera, K. S. Scott, P. A. R. Ade, J. J. Bock, J. Glenn, S. R. Golwala, S. Kim, Y. Kang, D. Lydon, P. D. Mauskopf, C. R. Predmore, C. M. Roberts, K. Souccar, and M. S. Yun, "The AzTEC mm-wavelength camera," *Monthly Notices of the Royal Astronomical Society* **386**, pp. 807–818, MAY 11 2008.
- [9] F. Piacentini, P. Ade, R. Bhatia, J. Bock, A. Boscaleri, P. Cardoni, B. Crill, P. de Bernardis, H. Del Castillo, G. De Troia, P. Farese, M. Giacometti, E. Hivon, V. Hristov, A. Iacoangeli, A. Lange, S. Masi, P. Mauskopf, L. Miglio, C. Netterfield, P. Palangio, E. Pascale, A. Raccanelli, S. Rao, G. Romeo, J. Ruhl, and F. Scaramuzzi, "The BOOMERANG North America instrument: A balloon-borne bolometric radiometer optimized for measurements of cosmic background radiation anisotropies from 0. degrees 3 to 4 degrees," *Astrophysical Journal Supplement Series* **138**, pp. 315–336, FEB 2002.
- [10] S. Masi, P. A. R. Ade, J. J. Bock, J. R. Bond, J. Borrill, A. Boscaleri, P. Cabella, C. R. Contaldi, B. P. Crill, P. de Bernardis, G. De Gasperis, A. de Oliveira-Costa, G. De Troia, G. Di Stefano, P. Ehlers, E. Hivon, V. Hristov, A. Iacoangeli, A. H. Jaffe, W. C. Jones, T. S. Kisner, A. E. Lange, C. J. MacTavish, C. M. Bettolo, P. Mason, P. D. Mauskopf, T. E. Montroy, F. Nati, L. Nati, P. Natoli, C. B. Netterfield, E. Pascale, F. Piacentini, D. Pogosyan, G. Polenta, S. Prunet, S. Ricciardi, G. Romeo, J. E. Ruhl, P. Santini, M. Tegmark, E. Torbet, M. Veneziani, and N. Vittorio, "Instrument, method, brightness, and polarization maps from the 2003 flight of BOOMERanG," *Astronomy & Astrophysics* **458**, pp. 687–716, NOV 2006.
- [11] J.-M. Lamarre, J. L. Puget, M. Piat, P. A. R. Ade, A. E. Lange, A. Benoit, P. De Bernardis, F. R. Bouchet, J. J. Bock, F. X. Desert, R. J. Emery, M. Giard, B. Maffei, J. A. Murphy, J.-P. Torre, R. Bhatia, R. V. Sudiwala, and V. Yourchenko, "Planck high-frequency instrument," in *IR Space Telescopes and Instruments. Edited by John C. Mather . Proceedings of the SPIE, Volume 4850, pp. 730-739 (2003).*, J. C. Mather, ed., Presented at the Society of Photo-Optical Instrumentation Engineers (SPIE) Conference **4850**, pp. 730–739, Mar. 2003.
- [12] A. Turner, J. Bock, J. Beeman, J. Glenn, P. Hargrave, V. Hristov, H. Nguyen, F. Rahman, S. Sethuraman, and A. Woodcraft, "Silicon nitride micromesh bolometer array for submillimeter astrophysics," *Applied Optics* **40**, pp. 4921–4932, OCT 1 2001.
- [13] P. D. Mauskopf, J. J. Bock, H. del Castillo, W. L. Holzapfel, and A. E. Lange, "Composite infrared bolometers with Si 3 N 4 micromesh absorbers," *Applied Optics* **36**, pp. 765–771, Feb. 1997.
- [14] K. Irwin and G. Hilton, "Transition-edge sensors," *Cryogenic Particle Detection* **99**, pp. 63–149, 2005.
- [15] K. Schwab, E. Henriksen, J. Worlock, and M. Roukes, "Measurement of the quantum of thermal conductance," *Nature* **404**, pp. 974–977, APR 27 2000.
- [16] H. Hoevers, M. Ridder, A. Germeau, M. Bruijn, P. de Korte, and R. Wiegink, "Radiative ballistic phonon transport in silicon-nitride membranes at low temperatures," *Applied Physics Letters* **86**, JUN 20 2005.
- [17] D. Anghel, J. Pekola, M. Leivo, J. Suoknuuti, and M. Manninen, "Properties of the phonon gas in ultrathin membranes at low temperature," *Physical Review Letters* **81**, pp. 2958–2961, OCT 5 1998.
- [18] W. Holmes, J. Gildemeister, P. Richards, and V. Kotsubo, "Measurements of thermal transport in low stress silicon nitride films," *Applied Physics Letters* **72**, pp. 2250–2252, MAY 4 1998.
- [19] K. Schwab, W. Fon, E. Henriksen, J. Worlock, and M. Roukes, "Quantized thermal conductance: measurements in nanostructures," *Physica B* **280**, pp. 458–459, MAY 2000.
- [20] W. Fon, K. Schwab, J. Worlock, and M. Roukes, "Nanoscale, phonon-coupled calorimetry with sub-attojoule/Kelvin resolution," *Nano Letters* **5**, pp. 1968–1971, OCT 2005.
- [21] M. Kenyon, P. K. Day, C. M. Bradford, J. J. Bock, and H. G. Leduc, "Electrical properties of background-limited membrane-isolation transition-edge sensing bolometers for Far-IR/Submillimeter direct-detection spectroscopy," *Journal of Low Temperature Physics* **151**, pp. 112–118, APR 2008.
- [22] W. Fon, K. Schwab, J. Worlock, and M. Roukes, "Phonon scattering mechanisms in suspended nanostructures from 4 to 40 K," *Physical Review B* **66**, JUL 15 2002.
- [23] M. Kenyon, P. K. Day, C. M. Bradford, J. J. Bock, and H. G. Leduc, "Electrical properties of background-limited membrane-isolation transition-edge sensing bolometers for Far-IR/Submillimeter direct-detection spectroscopy," *Journal of Low Temperature Physics* **151**, pp. 112–118, APR 2008.
- [24] Z. Moktadir, M. Bruijn, R. Wiegink, M. Elwenspoek, M. Ridder, and W. Mels, "Limitations of heat conductivity in cryogenic sensors due to surface roughness [x-ray detection]," *Sensors, 2002. Proceedings of IEEE* **2**, pp. 1024–1027 vol.2, June 2002.

- [25] B. Zink and F. Hellman, "Specific heat and thermal conductivity of low-stress amorphous Si-N membranes," *Solid State Communications* **129**, pp. 199–204, JAN 2004.
- [26] R. Welty and J. Martinis, "A series array of dc squids," *Magnetics, IEEE Transactions on* **27**, pp. 2924–2926, Mar 1991.
- [27] R. Cantor, L. Lee, A. Matlashov, and V. Vinetskiy, "A low-noise, two-stage dc squid amplifier with high bandwidth and dynamic range," *Applied Superconductivity, IEEE Transactions on* **7**, pp. 3033–3036, Jun 1997.
- [28] T. Kuhn, D. Anghel, J. Pekola, M. Manninen, and Y. Galperin, "Heat transport in ultrathin dielectric membranes and bridges," *Physical Review B* **70**, SEP 2004.
- [29] P. G. Murphy and J. E. Moore, "Coherent phonon scattering effects on thermal transport in thin semiconductor nanowires," *Physical Review B* **76**, OCT 2007.
- [30] K. Saito and A. Dhar, "Fluctuation theorem in quantum heat conduction," *Physical Review Letters* **99**, NOV 2 2007.
- [31] H.-Y. Zhang, H.-J. Li, W.-Q. Huang, and S.-X. Xie, "Acoustic phonon transport through a quantum waveguide with two stubs," *Journal of Physics D-Applied Physics* **40**, pp. 6105–6111, OCT 7 2007.
- [32] L. Jian-Duo, S. Liang, H. Yang-Lai, and Y. Lin, "Phonon transport and thermal conductivity in an acoustic filter," *Chinese Physics Letters* **24**, pp. 793–796, MAR 2007.
- [33] Y. Ming, Z. Wang, and Z. Ding, "Acoustic phonon transport through a double-bend quantum waveguide," *Physics Letters A* **350**, pp. 302–308, FEB 6 2006.
- [34] G. Palasantzas, "Ballistic thermal conductance limited by phonon roughness scattering: A comparison of power-law and Gaussian roughness," *Physical Review B* **70**, OCT 2004.